Estimating the mass eruption rate of volcanic eruptions from the plume height using Bayesian regression with historical data: the MERPH model

Mark J. Woodhouse

School of Earth Sciences
University of Bristol
Wills Memorial Building
Bristol BS8 1RJ
UK

mark.woodhouse@bristol.ac.uk

This paper is a non-peer reviewed preprint submitted to EarthArXiv.
The preprint has been submitted Journal of Volcanology and Geothermal Research for peer review.

Highlights

Estimating the mass eruption rate of volcanic eruptions from the plume height using Bayesian regression with historical data: the MERPH model

Mark J. Woodhouse

- A Bayesian linear regression is applied to eruption source parameter datasets
- Inference of mass eruption rate from plume height can be obtained with a quantification of uncertainty
- Analytical forms for the Posterior Predictive distributions facilitate analysis and sampling
- Observational uncertainty can be included in prediction

Estimating the mass eruption rate of volcanic eruptions from the plume height using Bayesian regression with historical data: the MERPH model

Mark J. Woodhouse

School of Earth Sciences, University of Bristol, Queens Road, Bristol, BS8 1RJ, , UK

Abstract

The mass eruption rate (MER) of an explosive volcanic eruption is a commonly used quantifier of the magnitude of the eruption, and estimating it is importance in managing volcanic hazards. The physical connection between the MER and the rise height of the eruption column results in a scaling relationship between these quantities, allowing one to be inferred from the other. Eruption source parameter datasets have been used to calibrate the relationship, but the uncertainties in the measurements used in the calibration are typically not accounted for in applications. This can lead to substantial over- or under-estimation. Here we apply a simple Bayesian approach to incorporate uncertainty into the calibration of the scaling relationship using Bayesian linear regression to determine probability density functions for model parameters. This allows probabilistic prediction of mass eruption rate given a plume height observation in a way that is consistent with the data used for calibration. By using non-informative priors, the posterior predictive distribution can be determined analytically. The methods and dataset are collected in a python package, called merph, and we illustrate their use in sampling plausible MER–plume height pairs, and in identifying usual eruptions. We discuss applications to ensemble-based hazard assessments and potential developments of the approach.

Keywords: Mass eruption rate, Plume height, Uncertainty quantification,, Bayesian regression

1. Introduction

The mass eruption rate (MER, denoted throughout by Q) of an explosive volcanic eruption is a quantity of fundamental importance in volcanology. The MER is often used (along with other quantities) to classify the strength of an eruption (Walker, 1980; Bonadonna and Costa, 2013; Pyle, 2015). During eruptions, rapid estimation of the MER is important for predicting hazards and monitoring evolution of the activity. The MER is an essential input to volcanic tephra transport and deposition models that forecast the dispersion of volcanic ash in the atmosphere (Mastin et al., 2009; Folch, 2012).

A common approach for making rapid estimates of the MER is to use an empirical algebraic expression relating MER to the plume height (denoted here by H). Data from historical eruptions, where there are independent estimates of the MER and plume height, have been compiled since the 1978 papers of Settle (1978) and Wilson et al. (1978) that gathered data to support the application of theoretical models of buoyant convection (Morton et al., 1956) to volcanic eruptions. While relatively small datasets ($n = 6$ eruptions in Settle 1978 and $n = 8$ eruptions in Wilson et al. 1978), the eruption MER spanned several orders of magnitude, with corresponding plume heights from the low troposphere to the high stratosphere. In the following decades these catalogues have been extended and revised, notably in Sparks (1986) ($n = 8$ eruptions), Sparks et al. (1997) ($n = 28$), Mastin et al. (2009) ($n = 35$) and Aubry et al. (2021) ($n = 130$).

The eruption datasets can be used to calibrate the parameters in a regression model. In both Sparks et al. (1997) and Mastin et al. (2009) a power-law relationship is used to model the dependence of the plume height on the MER, i.e. $Q = 10^{\alpha} H^{\beta}$, and the fitting parameters α and β are found from linear regression of $x = \log H$ and $y = \log Q$ with the observational dataset. This form is consistent with theoretical models of buoyant turbulent convection in a linear stable stratification, where the exponent $\beta = 4$ (Morton et al., 1956). The curves obtained by regression, shown in figure 1, describe the leading-order behaviour seen in the data, but there is substantial scatter of the data points around the calibrated relationship. Indeed, there are eruptions in these datasets that have a measured MER that differs by in excess of one order-of-magnitude from the power-law prediction. In applications, an order-of-magnitude under- or over-prediction of the MER could greatly limit the predictive ability of a dispersion model or inferences of changes in eruptive behaviour.

It is possible to obtain confidence intervals on the fitting parameters in the model relationship using linear regression of the log-transformed data (Mastin et al., 2009; Aubry et al., 2021, 2023). While this can be used to account for some of the scatter in the data, it does not fully account for the uncertainty in the observational data or in the model relationship used to describe it. There have recently been attempts to incorporate uncertainties into the eruption datasets (Aubry et al., 2021) and to consider model un-

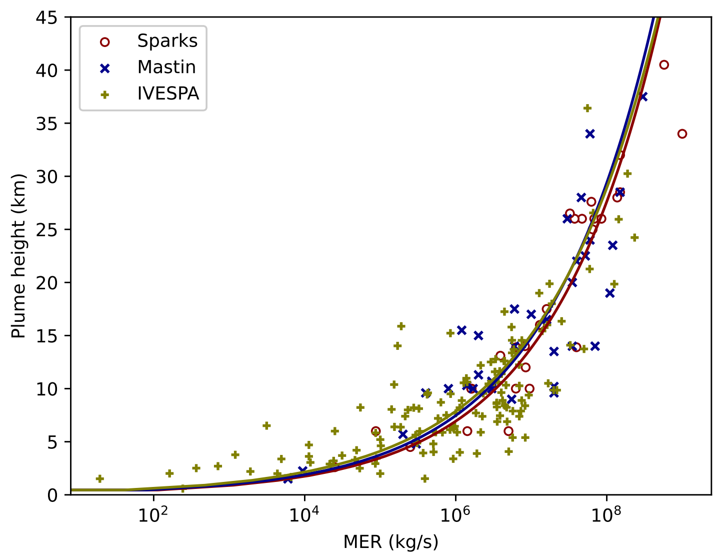

Figure 1: The eruption datasets of Sparks et al. (1997), Mastin et al. (2009) and IVESPA (Aubry et al., 2021), with corresponding power-law regression curves obtained from ordinary least squares linear regression of the log-transformed data.

certainties in the application of the relationship using stochastic modelling (Sparks et al., 2024). Here we present a structured approach using Bayesian methods to are widely used to quantify uncertainties,

Bayesian methods allow us to incorporate a range of uncertainties quantitatively into our model, and provide a meaningful way to quantitatively compare different models (e.g. Gelman et al., 2014). A Bayesian calibration of a model allows us to make probabilistic predictions, and identify outliers in the data (and so determine, quantitatively, whether an eruption is unusual). Importantly, with probabilistic information built into the predictive model, we are able to draw samples and build ensembles of plausible MER–plume height pairs (e.g. a set of plausible MERs corresponding to a height observation) each with an associated probability. This could allow for ensemble simulation of atmospheric tephra dispersion with inputs drawn in a structured way from distributions, facilitating the production of probabilistic forecasts.

In this paper we present a Bayesian approach, Bayesian linear regression, which is a standard method in statistical modelling (e.g. Gelman et al., 2014). This contribution illustrates and discusses the application to modelling the relationship between MER and plume heights using eruption source parameter datasets. In our application of the methodology, the statistical model of the observations has a simple form, assuming the 'errors' in the data do not depend on the observations and are independent and identically distributed. This allows the calculations needed to calibrate model parameters and to perform prediction with the fitted model to be performed analytically. The resulting posterior predictive distribution is a well-known distribution (the

t-distribution) and therefore subsequent computations can be performed using standard numerical libraries. More complicated statistical models could be applied, and we discuss extensions of the statistical model proposed, but likely require the use of numerical methods (such as Markov Chain Monte Carlo) to approximate the posterior distributions of the model parameters and the posterior predictive distribution.

Our contribution is structured as follows. In §2 we introduce three eruption source parameter datasets considered here, and present our statistical model to relate MER and plume height. We present the analytical formulae for the posterior distributions of the model parameters and, most importantly, the posterior predictive distribution. We illustrate the use of the statistical model in §3, considering inference of unobserved quantities, identification of unusual events, and incorporation of measurement uncertainty. In §4 we discuss the limitations and extensions of the statistical model, and the application of the Bayesian approach to ensemble based modelling, before presenting our conclusion in §5.

The methods developed here have been implemented in the Python package, MERPH, available from the PyPi package manager (https://pypi.org/project/merph/). This package includes the three datasets, as well as functionality to use alternative data sets. Each of the results illustrated below can be easily computed using MERPH, and the package includes an interactive Jupyter notebook to illustrate the application.

2. Methods

2.1. Eruption source parameter datasets

We use the eruption source parameter datasets of Sparks et al. (1997), Mastin et al. (2009) and Aubry et al. (2021). The datasets do not all contain the same eruptions, and may distinguish phases of some eruptions. Furthermore, the development over time has increased the number of eruption and atmospheric '*features*' that are recorded in the datasets. This could facilitate segregation of the data, but here we retain the complete datasets.

The dataset of Sparks et al. (1997) extents the catalogues of Settle (1978) and Wilson et al. (1978), with 28 eruptions at 18 volcanoes, recording the source volume flux, column height (above vent elevation) and (in 21 cases) the duration of the eruption (or phase of eruption). Sparks et al. (1997) notes substantial uncertainties implicit in both the column height and volume flux, but also that the studies from which the data derive typically do not quantify the uncertainties. In four eruptions a range of the volume flux is given, while 11 have a range of values of the column height. In these cases, we adopt the mid-point of the range. Using a density of 2500 kg/m^3, a dense rock equivalent mass eruption rate is computed from the volume flux.

The power-law curve fit obtained from regression using the data of Mastin et al. (2009), commonly known as 'the Mastin curve', is frequently used in tephra dispersion modelling. The dataset contains 35 eruptions from 19 volcanoes, spanning a period from 1902 to 2005. Mastin et al. (2009) present their dataset with eruptions separated into *'Silicic and andesitic eruptions'* (with 28 eruptions) and *'Basaltic eruptions'* (with seven eruptions). Each eruption has a plume height (above vent elevation), erupted volume, MER and duration. Eight of the plume heights are presented as a range of values; in these cases we adopt the mid-point value. Four eruptions have a range for the MER, and we take the mid-point value. Additional features in the dataset include the magma type and the Volcanic Explosivity Index (VEI) of an eruption (which is cumulative for eruptions separated into phases). Furthermore, the plume height observations are associated with an observation method.

The IVESPA dataset (Aubry et al., 2021) has substantially increased the number of events (i.e., eruptions and phases of eruptions) to 137. These events correspond to 68 eruptions at 45 volcanoes (according to Global Volcanism Program 2023). There are also many more features recorded that in the earlier datasets. For example, IVESPA includes three features that could be used to quantify the plume height: *'Tephra plume top height'* (which we adopt here), *'Spreading height of the Umbrella Cloud'*, and *'SO_2 plume height'*. Aubry et al. (2023) discuss the differences in curve fits obtained when using these different features to represent the plume height. The plume heights in IVESPA are given above sea level, so for consistency with the Sparks et al. (1997) and Mastin et al. (2009) dataset and the basis of the power-law model, we convert to heights above the vent using vent elevations contained in IVESPA. A few events do not have a plume height recorded, and these must therefore be excluded from our analysis, resulting in a dataset with 130 events. The MER is not recorded in IVESPA, so here is computed from the *'Tephra Erupted Mass'* and *'Duration'* features. The means that the MER is an average over the duration of the eruption, which is consistent with the data in the Sparks et al. (1997) and Mastin et al. (2009) datasets.

IVESPA also includes estimates of the uncertainty in the quantities that could be included in a statistical analysis, but in this study we do not include these uncertainties.

2.2. The statistical model

The leading-order behaviour in the observational data can be described by a power-law relationship, and dimensional reasoning supports the power-law dependence (Morton et al., 1956; Sparks et al., 1997). Therefore, we first make a logarithmic transformation of the data.

Here we present the method assuming that the plume height H is observed, and we seek to infer MER Q, as this is the practical use envisaged for emergency response. However, the method can be used with the roles of these variables switched (i.e. H as a function of Q), which may be useful for preparatory modelling and risk analysis, with only changes in the numerical values that are computed and the interpretation of the results.

Taking logarithms of the data, we write $x_i = \log H_i$ as the 'explanatory' variable and $y_i = \log Q_i$ as the 'response' variable, where (H_i, Q_i) is the pair of observed plume height (in km above the vent) and mass eruption rate (in kg/s) for eruption i in a historical record containing n eruptions. (Strictly, the plume height and MER should be non-dimensionalized before taking the logarithm, and so implicitly we have non-dimensionalized heights using a length scale of 1 km, and the MER by 1 kg/s.) The leading order power-law relationship between Q and H suggests $\mathbb{E}\left(y_i\right) = \alpha + \beta x_i$, where $\mathbb{E}\left(\cdot\right)$ denotes the expectation, so that our statistical model for the logarithmically transformed data is

$$y_i = \alpha + \beta x_i + \epsilon_i, \tag{1}$$

where ϵ_i is the error in the observation of eruption i which includes contributions from aleatoric variations, measurement uncertainty and unmodelled process.

Examples of unmodelled processes are varying atmospheric conditions that are not accounted for in our simple relationship (e.g. wind, which is known to strongly influence the plume dynamics, e.g. Bursik, 2001; Degruyter and Bonadonna, 2012; Woodhouse et al., 2013; Aubry et al., 2023), and volcanological parameters than are not explicitly included (e.g. physical properties of the magma, conduit geometry etc.) but which may alter the relationship. The measurement uncertainty includes both instrumental errors, recording errors, and errors in the derivation of the MER from tephra deposit volume and eruption duration.

As there are several contributions to the error term, and the eruptions in the databases are located across the world and span several decades, it is reasonable to assume that the errors for each event are independent. Furthermore, we assume that the error does not depend on the size of the eruption or the plume height. Therefore, we take the errors to be independent and identically distributed, with $\epsilon_i \sim N(0, \sigma^2)$ where $N(\mu, \sigma^2)$ denotes the Normal distribution with mean μ and variance σ^2. The assumption of homoscedasticity (i.e., an equal error variance for each eruption) is discussed further below. We note that σ^2 is unspecified and must be estimated as part of model calibration.

We are required to determine the three parameters in the statistical model, with $\alpha \in \mathbb{R}$, $\beta \in \mathbb{R}$ and $\sigma^2 > 0$. These parameters are estimated using Bayesian linear regression (Gelman et al., 2014). For ease of notation, we define a $(2 \times n)$ matrix X as

$$\mathrm{X}^T = \begin{pmatrix} 1 & 1 & \dots & 1 \\ x_1 & x_2 & \dots & x_n \end{pmatrix} \tag{2}$$

and the vector of fit parameters $\boldsymbol{\beta} = (\alpha, \beta)^T$. The mean of $\boldsymbol{x}$ is $\bar{\boldsymbol{x}} = \frac{1}{n}\sum x_i$, and $\mathrm{var}(\boldsymbol{x})$ denotes the variance of the $\boldsymbol{x}$ data (and similarly for $\boldsymbol{y}$).

2.3. Maximum likelihood estimators

Under the statistical model proposed, the likelihood is

$$\boldsymbol{y} \mid \boldsymbol{\beta}, \sigma^2, \mathrm{X} \sim N\left(\mathrm{X}\boldsymbol{\beta}, \sigma^2 \mathrm{I}\right), \tag{3}$$

where I denotes the $n \times n$ identity matrix. From this we obtain the maximum likelihood estimators

$$\widehat{\boldsymbol{\beta}} = \mathrm{V}\mathrm{X}^T\boldsymbol{y}, \quad \text{and} \quad \widehat{\sigma}^2 = \frac{1}{n-2}\left(\boldsymbol{y} - \mathrm{X}\widehat{\boldsymbol{\beta}}\right)^T\left(\boldsymbol{y} - \mathrm{X}\widehat{\boldsymbol{\beta}}\right), \tag{4}$$

where

$$\mathrm{V} = \left(\mathrm{X}^T\mathrm{X}\right)^{-1} = \frac{1}{n^2 \mathrm{var}\left(\boldsymbol{x}\right)} \begin{pmatrix} \sum_{i=1}^{n} x_i^2 & -\sum_{i=1}^{n} x_i \\ -\sum_{i=1}^{n} x_i & n \end{pmatrix}. \tag{5}$$

Note, from (4) we find

$$\widehat{\beta} = \frac{\mathrm{cov}\left(\boldsymbol{x}, \boldsymbol{y}\right)}{\mathrm{var}\left(\boldsymbol{x}\right)}, \tag{6}$$

$$\widehat{\alpha} = \bar{\boldsymbol{y}} - \widehat{\beta}\bar{\boldsymbol{x}}, \tag{7}$$

and $\widehat{\sigma}^2$ is the mean square error of the data. These are the same values of the 'best fit' model parameters that would be found from an ordinary linear regression of the log-transformed data.

2.4. Probability distributions for model parameters

To incorporate the uncertainty in the observations and the uncertainty due to limitations of the model, we seek to obtain probability distributions on the parameters in the model. This is achieved through a Bayesian approach, where prior probability distributions are assigned to the model variables based on our beliefs about their values, and these prior probabilities are updated using Bayes' theorem with the information contained in the set of observations. Here we take a standard non-informative prior assuming $\boldsymbol{\beta}$ and σ^2 are independent, known as the Jeffrey's prior, which has the form

$$p\left(\boldsymbol{\beta}, \sigma^2 \mid \mathrm{X}\right) \propto 1/\sigma^2. \tag{8}$$

If σ^2 were known, then the posterior distribution of $\boldsymbol{\beta}$ could be obtained. However, since σ^2 is not known, instead we can write the conditional posterior distribution of $\boldsymbol{\beta}$ given σ^2, which is

$$\boldsymbol{\beta} \mid \sigma^2, \boldsymbol{y}, \mathrm{X} = N\left(\widehat{\beta}, \mathrm{V}\sigma^2\right). \tag{9}$$

The marginal posterior of σ^2 with the non-informative prior is given by

$$\sigma^2 \mid \boldsymbol{y}, \mathrm{X} = IG\left(\left(n-2\right)/2, (n-2)\widehat{\sigma}^2/2\right), \tag{10}$$

where IG is the inverse-Gamma distribution.

If needed, values of the model parameters can be obtained by drawing from these distributions, i.e., first a value of the error term variance is drawn from the inverse-Gamma distribution using (10), which can then be used in (9) and values of α and β obtained by draws from the multivariate Normal distribution. This then gives alternative curve-fits that are feasible given the data. A credible interval for the curve fit can be found from the posterior distribution of y, which has the form of a non-standardized t-distribution,

$$y_j = \alpha + \beta x_j \sim t_{n-2}\left(\widehat{\alpha} + \widehat{\beta} x_j, \widehat{\sigma}^2 \left[\frac{1}{n} + \frac{(x_j - \bar{x})^2}{n\mathrm{var}\,(\boldsymbol{x})}\right]\right). \tag{11}$$

Note, for this simple model, the credible interval is numerically the same as a confidence interval for the regression line, although the interpretation is different (see e.g. Lu et al., 2012).

These posterior distributions, and samples or statistics derived from them, characterize the uncertainty in the statistical model, given the data. However, they are typically not needed in the practical applications. Instead, we wish to use the uncertainty in the model parameters, now quantified in the posterior distributions, to provide probabilistic predictions of the response variable when a new observation of the explanatory variable is made.

2.5. Posterior prediction

The posterior distribution of the model parameters can be used to draw sample sets of model parameters that are consistent with the data. If, during an eruption, a new observation of the plume height is made, and therefore a new explanatory variable $\tilde{x}$ is given, we can use the posterior distribution of the model parameters to predict a distribution of values for the MER that are consistent with the new observation, the data underlying the curve-fit, and the uncertainties in the data and the model.

Under the statistical model, if the model parameters were known precisely, then we have

$$\tilde{y} \sim N\left(\alpha + \beta\tilde{x}, \sigma^2\right). \tag{12}$$

The uncertainty in the observations and the model is incorporated through the posterior distributions of the model parameters α, β and σ^2. When including these uncertainties, we arrive at the posterior predictive distribution, $p\left(\tilde{y} \mid \tilde{x}, \boldsymbol{y}, \mathrm{X}\right)$. This can be obtained by simulation, by drawing many samples from the posterior predictive distribution by first sampling the model parameters from their posterior distributions, and then using these as fixed values in equation (12). However, for our simple model and choice of non-informative prior, the posterior distribution can be written analytically (see Gelman et al., 2014, for details) as

$$\tilde{y} \mid \tilde{x}, \boldsymbol{y}, \boldsymbol{x} \sim t_{n-2}\left(\widehat{\alpha} + \widehat{\beta}\tilde{x}, \widehat{\sigma}^2\left[1 + \frac{1}{n} + \frac{\left(\tilde{x} - \bar{x}\right)^2}{n\mathrm{var}\left(\boldsymbol{x}\right)}\right]\right), \tag{13}$$

a t-distribution with $n-2$ degrees-of-freedom, with location at the log-MER predicted by the maximum likelihood estimate at the observed plume height, and a scale parameter that incorporates the estimated measurement uncertainty through the maximum likelihood estimate of the error variance. Note, the scale parameter for the posterior predictive distribution is larger than the scale parameter for the posterior distribution for the curve fit, equation (11), which accounts for the uncertainty of a new observation around the curve fit.

The logarithmic transformation can be inverted, so that the posterior predictive distribution for the MER given a new plume height observation and a historical dataset is a log-t distribution.

If multiple new height observations are made, so we have a vector of new explanatory variables $\tilde{\boldsymbol{x}}$, then the posterior predictive distribution of $\tilde{y}$ is found as a multivariate t-distribution, with

$$\tilde{y} \mid \tilde{x}, \boldsymbol{y}, \boldsymbol{x} \sim t_{n-2}\left(\widetilde{\mathrm{X}}\widehat{\beta}, \widehat{\sigma}^2\left[\mathrm{I} + \widetilde{\mathrm{X}}\mathrm{V}\widetilde{\mathrm{X}}^T\right]\right). \tag{14}$$

However, the typical case will be a single new observation.

We note that the analytical form of the posterior predictive distribution is a major advantage, as it allows samples to be drawn from the distribution very easily. The t-distribution is commonly used in statistical analysis, so there are many software packages that provide algorithms for computing quantities (such as the CDF and quantiles) from the t-distribution (e.g., the scipy package in Python, the Statistics and Machine Learning Toolbox in MatLab, and in R). Furthermore, the location and scale parameters in the t-distribution can be computed directly from the maximum likelihood estimates for the model parameters and other quantities of the data.

2.6. Including observational uncertainty in predictions

The posterior predictive distribution in (13) assumes that the observation is exact. In applications where a plume height is observed, there is likely to be an associated uncertainty. We can characterize this uncertainty through a probability distribution for the new observation, $p(\tilde{x})$, and the joint posterior predictive distribution can be computed using

$$p(\tilde{x}, \tilde{y}|\boldsymbol{x}, \boldsymbol{y}) = p(\tilde{y}|\tilde{x}, \boldsymbol{x}, \boldsymbol{y})p(\tilde{x}) \tag{15}$$

which allows samples to be drawn using equation (13).

3. Results

Here we illustrate the application of the Bayesian regression using the datasets of Sparks et al. (1997), Mastin et al. (2009) and IVESPA (Aubry et al., 2021).

3.1. Maximum likelihood estimators and posterior distributions for model parameters

The maximum likelihood estimators of the model parameters, computed from (4) for each dataset, are tabulated in table 1. These give the 'best-fit' curves for each dataset, which we refer to as the 'Sparks curve', 'Mastin curve' and 'IVESPA curve', for the Sparks et al. (1997), Mastin et al. (2009) and IVESPA (Aubry et al., 2021) datasets, respectively. The power-law exponent, $\widehat{\beta}$, differs only slightly for each of the three datasets (table 1), but there are more substantial differences between the maximum likelihood estimates of the pre-factor $\widehat{\alpha}$. However, these differences do not strongly alter the curves (figure 1).

It is noteworthy that the magnitude of the uncertainty, encapsulated in the variance of the normally-distributed error term, $\widehat{\sigma}^2$, increases markedly as the size of the dataset increases (table 1). This indicates that the increasing size of the historical record is capturing a larger range of eruption and atmospheric conditions, so the scatter of data points around the best-fit curve increases, as seen in figure 1.

Dataset	n	$\widehat{\alpha}$	$10^{\widehat{\alpha}}$	$\widehat{\beta}$	$\widehat{\sigma}^2$
Sparks	28	2.99	981.84	3.47	0.11
Mastin	35	3.07	1164.24	3.36	0.22
IVESPA	130	2.83	668.99	3.54	0.59

Table 1: Maximum likelihood estimates for the model parameters $\widehat{\alpha}$ and $\widehat{\beta}$ for the model $Q = 10^{\alpha} H^{\beta}$, found from log-transformation of the data of Sparks et al. (1997), Mastin et al. (2009) and IVESPA (Aubry et al., 2021). The size of the dataset, n, is also given.

The posterior distributions for the model parameters are given in equations (9) and (10) and can be used to sample curves that fit the data. In figure 2 the curves obtained from 100 random samples from the posterior distributions of the model parameters using the Mastin et al. (2009) data are shown together with data, the Mastin curve obtained from maximum likelihood estimation and the 95% credible interval of the best fit curve. Note the 95% credible interval indicates the region where we have high belief in the curve fit; there is a probability of 0.95 that the 'true' best-fit curve lies within the credible interval.

3.2. Posterior prediction

In applications, the posterior predictive distribution is used to determine estimates of the MER that are consistent with a new height observation and the data underlying the model. Table 2 presents values of the location and scale parameters in the posterior prediction distribution for the log-MER given a plume height observation in the range 5–50 km for the Sparks et al. (1997), Mastin et al. (2009) and IVESPA (Aubry et al., 2021) datasets. The location parameter values (given by $\mu = \widehat{\alpha} + \widehat{\beta}\tilde{x}$, which quantifies the

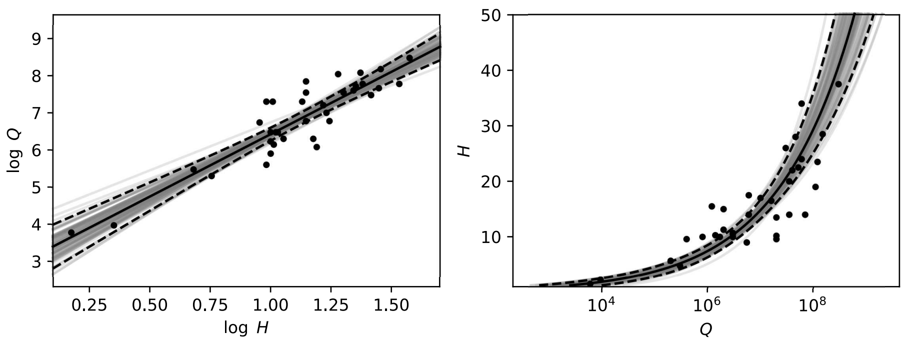

Figure 2: Possible curve fits to the Mastin et al. (2009) dataset obtained from sampling the posterior distributions of the model parameters. The left-hand panel shows the log-transformed data. The right-hand panel show the MER–plume height data as commonly plotted. The black solid lines show the 'best-fit' curve obtained from maximum likelihood estimation of the model parameters, with the black dashed lines showing the 95% confidence intervals on the curve fit. The semi-transparent grey lines show 100 alternative curve fits from sampling of the posterior distributions of the model parameters.

most likely log-MER) at each height are similar for each dataset, but the scale parameter (quantifying the variability around the maximum likelihood value) is substantially larger for the IVESPA dataset. For each dataset, the scale parameter varies only slightly over the large range of heights, increasing gradually with increasing distance of the observed log-plume height from the mean of the data, $|\tilde{x} - \bar{x}|$.

Figure 3 shows the posterior predictive distribution for the log-MER for three plume height observations, for each of the Sparks et al. (1997), Mastin et al. (2009) and IVESPA (Aubry et al., 2021) datasets. Here the larger variability in the IVESPA dataset is apparent. We also note that, for each dataset, the posterior predictive distributions for different height observations overlap. For example, using the Sparks et al. (1997) data, the most likely values of the MER for plume heights of 5, 10 and 20 km differ by a full decade

$\widetilde{H}$ (km)	$\widetilde{x}$	Sparks		Mastin		IVESPA	
		μ	τ	μ	τ	μ	τ
5	0.699	5.42	0.358	5.41	0.494	5.30	0.772
10	1.00	6.47	0.344	6.43	0.482	6.37	0.771
15	1.18	7.08	0.342	7.02	0.481	6.99	0.774
20	1.30	7.51	0.343	7.44	0.483	7.43	0.777
25	1.40	7.85	0.345	7.76	0.487	7.78	0.780
30	1.48	8.12	0.348	8.03	0.491	8.06	0.783
35	1.54	8.36	0.351	8.25	0.495	8.29	0.786
40	1.60	8.56	0.354	8.45	0.499	8.50	0.788
45	1.65	8.74	0.357	8.62	0.503	8.68	0.791
50	1.70	8.90	0.361	8.78	0.506	8.84	0.793

Table 2: Location (μ) and scale (τ) parameters in the posterior predictive distribution of the logarithm of the MER for specified plume heights, $\tilde{y} \sim t_{32}\left(\mu, \tau^2\right)$, using data from Sparks et al. (1997), Mastin et al. (2009) and IVESPA (Aubry et al., 2021).

(with $\log Q$ taking values of 5.42, 6.47 and 7.51, respectively), but from the posterior predictive distribution at these heights we find

$$\begin{aligned} &P(5.90 < \log Q < 6.00 | H = 5, \text{Sparks}) \\ &\quad \approx P(5.90 < \log Q < 6.00 | H = 10, \text{Sparks}) = 0.037 \end{aligned} \tag{16}$$

so that if we observe a plume at height 5 km, there is a probability of 3.7% that $\log Q \approx 5.95$, and the same MER is found with equal probability for a plume at height 10 km. The larger variability in the IVESPA data results in more pronounced overlapping of the posterior predictive distributions for different height observations. In this case,

$$\begin{aligned} &P(6.32 < \log Q < 6.42 | H = 5, \text{IVESPA}) \\ &\quad \approx P(6.32 < \log Q < 6.42 | H = 20, \text{IVESPA}) = 0.022 \end{aligned} \tag{17}$$

so there are appreciable probabilities of a MER with $\log Q \approx 6.37$ for plumes reaching 5 km or 20 km (noting this value for the MER is the most likely for plume reaching 15 km). Note this should not be interpreted to mean that there are equal probabilities (under the IVESPA model) for a plume height of 5 km and 20 km for a MER of $10^{6.37} = 2.34 \times 10^6$ kg/s; to determine these probabilities we need the posterior predictive distribution of the plume heights *given a MER*, from which we find that the most likely plume height is 9 km.

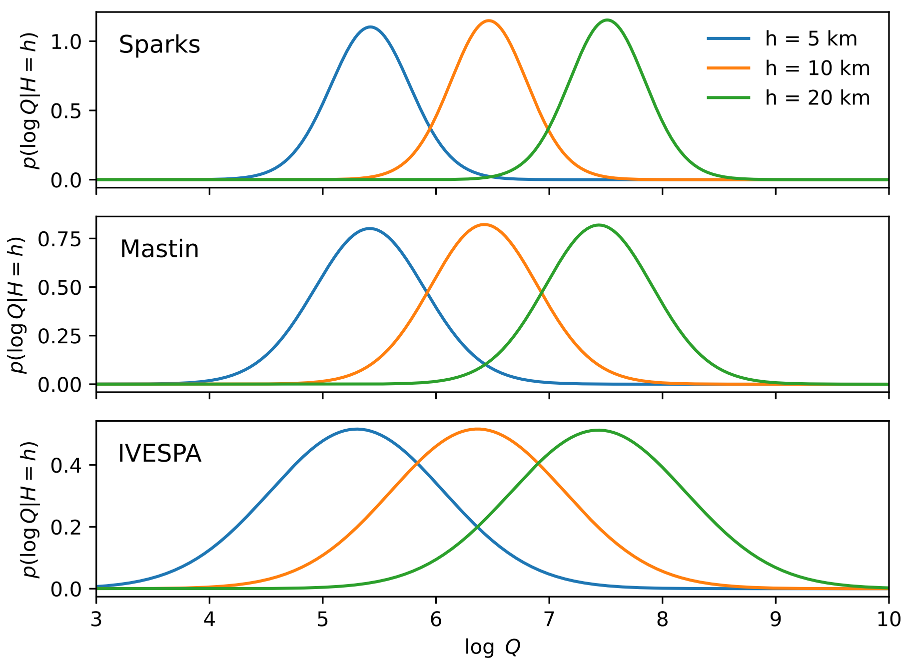

Figure 3: Posterior predictive densities, $p(\log Q\,|\log H = \log h, \boldsymbol{y}, \boldsymbol{x})$, for the Sparks et al. (1997), Mastin et al. (2009), and IVESPA (Aubry et al., 2021) datasets, for three plume heights observations: $h = 5$km, 10km, and 20km.

The posterior predictive distribution can be found for any new height observation. Figure 4 illustrates posterior prediction intervals using the Mastin et al. (2009) dataset for $\log Q | \log H$ for a range of plume heights, together with the data, the Mastin curve, and the 95% credible interval for the curve fit. The $(1-\alpha) \times 100\%$ posterior prediction interval is a centred interval satisfying $P(y_l < Y < y_u | X) = 1 - \alpha$ for a specified $0 < \alpha < 1$. Decreasing α produces wider bands, indicating a greater probability that the true MER lies within the prediction interval.

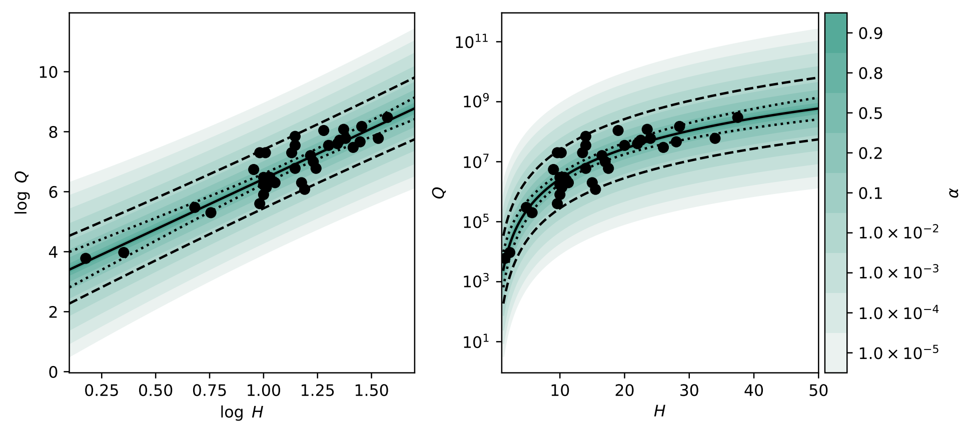

Figure 4: Posterior prediction intervals of the MER given a plume height observation for the Mastin et al. (2009) dataset (data indicated by black circles). The Mastin curve is indicated by the solid black line, with the 95% credible interval on the curve fit shown with dotted lines. The overlapping coloured bands indicate centred prediction intervals (i.e. curves $y_l(x)$ and $y_u(x)$ such that $P(y_l < Y < y_u | X) = 1 - \alpha$). The prediction interval for $1 - \alpha = 0.95$ is shown with dashed lines.

Figure 4 shows that the 95% predictive interval is much wider than the 95% credible interval for the curve fit, which we recall is numerically identical to a 95% confidence interval for the curve fit. Therefore, confidence intervals on the curve fit by themselves do not adequately capture the uncertainty when making predictions. The predictive distribution, with its greater variance, must be used when sampling plausible MER values based on plume height observations.

The contours of the intervals (in log-space) are slightly narrower where there are more data, although this is less apparent in the for the predictive intervals than for the credible interval on the curve fit (Figure 4). The illustrates that we have a stronger belief that the calibrated curve well represents the data in regions where the data is clustered, and less belief where there is sparse data. In contrast, the predictive interval captures the scatter in the data, so while there is most data for plumes are 11 km, there is considerable scatter in the MER for these eruptions, so wide prediction intervals are needed.

3.2.1. Identifying unusual eruptions

The posterior predictive distribution allows us to identify unusual events quantitatively. Methods have been developed to identify outliers within a dataset (e.g. Chaloner and Brant, 1988). Here we seek to determine whether a new eruption, not within a dataset but with a MER and plume height observation, is unusual. To illustrate this, we select eruptions from the IVESPA dataset (Aubry et al., 2021) that are not contained in the Mastin et al. (2009) dataset, and use the posterior predictive distributions derived from the Mastin et al. (2009) data to characterize these new events.

There are 29 eruptions in the IVESPA dataset that occurred since the publication of the Mastin et al. (2009) dataset. For each of these eruptions, we use the observations to produce posterior predictive distributions for both MER and plume height and compute the probability $P(\log 0.8 + y^* \leqslant Y \leqslant \log 1.2 + y^* | x^*, \boldsymbol{x}, \boldsymbol{y})$ for each, where x^* and y^* denote the observations (either

$\log Q$ or $\log H$) from IVESPA, i.e., we determine the probability that the posterior prediction lies within $\pm 20\%$ of the recorded observation. Table 3 shows these probabilities.

The four plumes of the 2015 eruption of Cotopaxi are notable for the low probabilities associated with the observed MER and plume heights, which suggest the eruption is unusual with respect to the Mastin et al. (2009) dataset. Indeed, for an observed plume height of 6.513 km, the Mastin regression would predict $P(Q \leqslant 3.14 \times 10^3) \approx 2 \times 10^{-5}$, and a MER more than order-of-magnitude larger than observed is required to reach the 1-percentile of the posterior predictive distribution. While the probabilities associated with predictions of the plume heights given the MER are larger, they remain relatively small.

The eruption of Etna, 21 May 2016, is also of interest, as the MER observation given the plume height might be considered unusual, with $P(Q < 7.1 \times 10^2 | H = 2.7) \approx 0.001$, but the plume height observation given the MER is not unlikely (the observed plume height of 4.7 km is less than 2 standard deviations from the mean of the posterior predictive distribution). This example illustrates the difference between the posterior predictive distributions for $\log Q | \log H$ and $\log H | \log Q$.

3.2.2. Joint predictive samples

Uncertainty in the observation can also be included, by sampling from the joint posterior predictive distribution using the decomposition given by equation (15). As an example, we consider here uncertain plume height observations, so that $H \in [h_0, h_1]$, and for illustration take a large range of possible values, $h_0 = 5$ km and $h_1 = 20$ km. We consider four distributions to characterize the uncertainty (referred to below as the 'measurement dis-

Eruption	Q^* (kg/s)	H^* (km)	$P_{Q^*\|H^*}$	$P_{H^*\|Q^*}$
Calbuco 22 April 2015	1.870×10^7	17.997	0.144	0.493
Calbuco 23 April 2015	1.275×10^7	18.997	0.123	0.417
Puyehue-Cordón Caulle layer A-F, 2011	4.630×10^6	10.330	0.134	0.433
Puyehue-Cordón Caulle layer H, 2011	4.012×10^6	9.630	0.129	0.406
Puyehue-Cordón Caulle layer K2, 2011	8.408×10^5	6.130	0.130	0.344
Cotopaxi 1st phase, 2015	3.135×10^3	6.513	**0.000**	**0.004**
Cotopaxi 2nd phase, 2015	3.664×10^2	2.513	**0.001**	0.071
Cotopaxi 3rd phase, 2015	1.624×10^2	2.013	**0.001**	0.084
Cotopaxi 4th phase, 2015	1.939×10^1	1.513	**0.000**	0.033
Etna 12 January 2011	2.510×10^4	6.000	**0.006**	0.124
Etna 23 February 2013	5.051×10^5	4.800	0.110	0.235
Etna 26 October 2013	1.136×10^4	4.700	**0.006**	0.159
Etna 23 November 2013	5.824×10^5	7.200	0.132	0.492
Etna 18 & 19 May 2016	1.907×10^3	2.200	0.027	0.391
Etna 21 May 2016	7.104×10^2	2.700	**0.001**	0.104
Eyjafjallajökull 14-16 April 2010	5.086×10^5	4.040	0.069	0.108
Eyjafjallajökull 17 April 2010	3.704×10^5	3.940	0.085	0.141
Eyjafjallajökull 18 April - 21 May 2010	8.617×10^4	2.940	0.116	0.190
Eyjafjallajökull 4-8 May 2010	8.951×10^4	3.440	0.136	0.314
Grímsvötn 21 May 2011	7.500×10^6	14.550	0.141	0.492
Kelut Unit B, 2014	5.938×10^7	21.269	0.127	0.483
Merapi 4 November 2010	1.698×10^5	14.032	**0.001**	0.011
Nakadake - Asosan 14 September 2015	1.000×10^5	1.998	0.031	0.017
Ontakesan 27 September 2014	4.630×10^4	3.275	0.131	0.402
Shinmoedake - Kirishimayaya Phase SP1+SP2, 2011	6.667×10^5	5.879	0.134	0.357
Shinmoedake - Kirishimayaya Phase SP3, 2011	3.333×10^5	5.979	0.134	0.477
Tungurahua 14 July 2013	1.867×10^5	6.377	0.083	0.450
Tungurahua 1 February 2014	3.488×10^6	8.677	0.116	0.345
Villarrica 3 March 2015	9.392×10^5	6.253	0.128	0.337

Table 3: Probabilities of eruption source parameters in the IVESPA dataset (Aubry et al., 2021) using the regression model for Mastin et al. (2009). The quantity $P_{Q^*|H^*}$ gives the probability $P(\log(0.8Q^*) < \log Q < \log(1.2Q^*)\,|H^*)$ and similarly for $P_{H^*|Q^*}$. Bold entries indicate eruptions where $P_{Q^*|H^*} < 0.01$ and/or $P_{H^*|Q^*} < 0.01$.

tributions' of the plume height): a uniform distribution, $H \sim U(h_0, h_1)$, and truncated normal distributions, $H \sim TN(\mu, \omega^2, h_0, h_1)$ with standard deviation ($\omega = 3$ km) taking mean at the centre of the interval ($\mu = 12.5$ km), a low-skewed mean ($\mu = 10$ km), and a high-skewed mean ($\mu = 15$ km). Figure 5 shows these probability distributions for the uncertain height observation together with the associated joint posterior predictive distributions $f_{Q,H}(q, h)$. Note, these distributions are given for the MER and plume height and not the logarithmically transformed variables, obtained by scaling equation (15), and this results in small values of the probability density due to the large range of values for the MER.

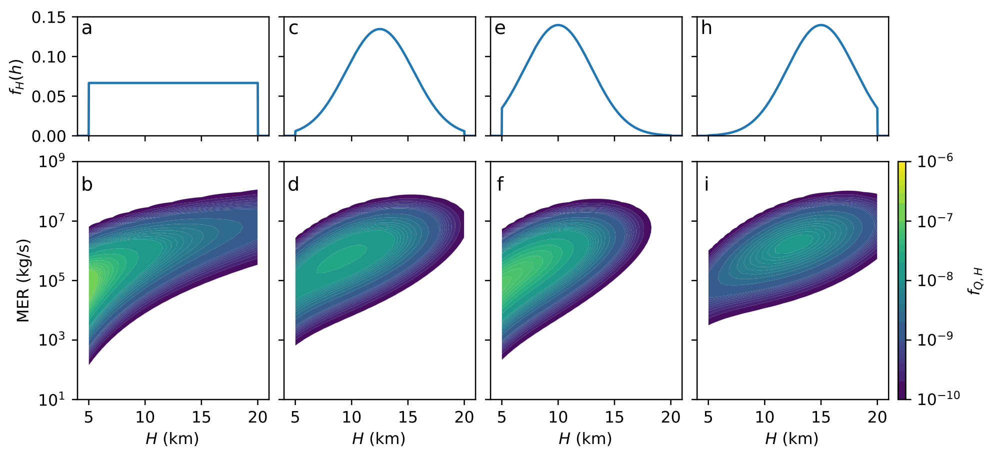

Figure 5: Joint posterior predictive distributions for the MER and plume height, based on uncertain plume height observations using the Mastin et al. (2009) dataset. The upper panels show the probability density function of the height observation, $f_H(h)$, and the lower panels show the associated joint posterior density distributions, $f_{Q,H}(q, h)$. (a,b) Uniform distribution, $H \sim U(5, 20)$. (c,d) Symmetric truncated normal distribution, $H \sim TN(12.5, 9, 5, 20)$. (e,f) Low-skewed truncated normal distribution, $H \sim TN(10, 9, 5, 20)$. (h,i) High-skewed truncated normal distribution, $H \sim TN(15, 9, 5, 20)$.

Each of the measurement distributions have finite domain, so curtail the joint distribution to this range of plume heights. For the uniform distribution (Figure 5a,b) the contours of the joint distribution resembles those of the prediction intervals of Figure 4. However, there is a noticeable asymmetry, with broader tails of probability density for small MER than large MER, and higher density for small plume heights than large. This is because the measurement distribution is not uniform in log-space and the posterior predictive distribution is not symmetric in linear space. The truncated normal distributions similarly do not produce symmetric joint distributions. The location of the maximum joint density moves with the maximum of the observed distribution, but is always offset to lower plume heights.

4. Discussion

4.1. Advantages, limitations and extensions

Bayesian linear regression of the MER and plume height in eruption databases provides a valuable methodology to interpret observations and to predict future eruption conditions. The model proposed here is arguably the simplest statistical model, but has some notable advantages. Firstly, the model produces an analytical result in the form of a well-known distribution (the t-distribution), so calculations can be performed easily. Secondly, the inference of model parameters from a dataset is straight-forward. Indeed, the model parameters of the posterior distribution are functions of quantities routinely computed in ordinary linear regression, consisting of the curve-fit parameters (slope and intercept) and the mean square error of the data. However, the simple approach has some limitations.

A key assumption of our statistical model is homoscedasticity (equal error variance for all observations). While this assumption allows us to obtain the analytical results, it also causes the inferred variance to be large in datasets where there is increased scatter. For example, in the IVESPA dataset (Aubry et al., 2021), there is substantially greater scatter of the observations around the MLE compared to the smaller Sparks et al. (1997) and Mastin et al. (2009) datasets (see figure 1 and table 1) so the posterior distribution for the error is wider in order to capture the observations using a normal distribution.

A heteroscedastic model, with an observation-specific error variance, may give improved fit to the observed data. Indeed, based on physical principles, we may wish to link the error variance to the explanatory variables. For example, transient weather conditions give highly variable wind and temperature in the troposphere, which can strongly impact plume dynamics (Bursik, 2001; Degruyter and Bonadonna, 2012; Woodhouse et al., 2013), and therefore greater aleatoric uncertainty for tropospheric plumes. Therefore, it may be appropriate to develop a statistical model allowing for larger error variance at low altitudes. This could be achieved either by using a functional relationship for the error variance, i.e., letting $\sigma_i = f(H_i)$, or by grouping events in the datasets into tropospheric and stratospheric eruptions. They may be additional grouping that could be applied, for example considering tropic, mid-latitude and high-latitude eruptions to assess the effect of eruption location.

More sophisticated statistical models could be applied, and there are likely to be benefits to this, particularly as eruption datasets grow, with more eruptions and more variables recorded. This would allow other controlling variables to be included in the regression analysis, to reduce epistemic uncertainties. For example, atmospheric effects could be included by incorporating a dependence of the plume height on the atmospheric stratification (quantified through the buoyancy frequency, N) and/or the wind speed; these variables and several others are included in the IVESPA dataset (Aubry et al., 2021).

Considering first the buoyancy frequency only, physical reasoning suggests the plume height scales as $H \sim N^{-3/4}Q^{1/4}$ (Wilson et al., 1978; Settle, 1978; Woods, 1988; Sparks et al., 1997; Degruyter and Bonadonna, 2012; Woodhouse et al., 2013). We can therefore retain a linear model in logarithmically transformed variables, albeit with in a model with two explanatory variables, so three fitting coefficients. The Bayesian linear regression can then be applied straight-forwardly (see Gelman et al., 2014).

In contrast, when modelling for the effect of wind speed, V, in integral plume models, Degruyter and Bonadonna (2012) and Woodhouse et al. (2013) suggest there is not a simple power-law dependence. Instead, the plume height scales as $H \sim N^{-3/4}Q^{1/4}f(\mathcal{W})$, where $\mathcal{W} = V/(HN)$ is a dimensionless wind speed, and where f is a decreasing function of $\mathcal{W}$. The functional forms proposed by Degruyter and Bonadonna (2012) and Woodhouse et al. (2013) differ, and we could base a new statistical model on these forms. However, in neither case do not obtain a linear model in logarithmic space, so the linear regression cannot be used. However, a nonlinear model could be used, with Markov Chain Monte Carlo methods used to fit and predict. This approach would also allow different functional forms to be tested and quantitatively compared.

The extension to model complex models may require computation. There are now several advanced toolkits for Probabilistic Programming (e.g., Abril-Pla et al., 2023; Stan Development Team, 2023) that provide easy-to-use interfaces to advanced computation methods for Bayesian inference. These methods allow non-specialists to implement models by specifying prior and likelihood functions directly as probability density functions linked to the data, and perform Markov Chain Monte Carlo integration to fit the model (i.e., numerically approximate the posterior distribution) and then make probabilistic predictions. Additionally, non-parametric approaches, such as Gaussian Process regression (e.g., Rasmussen and Williams, 2006) could be used to create models that do not rely on a pre-specified form for the relationship. This provides a more 'data-driven' approach by removing the need for an initial physics-based model on which to base the inference, but care must be taken to ensure physical laws are not violated by the resulting model.

4.2. Applications to tephra dispersion modelling

Estimates of MER and plume height are important inputs for tephra hazard simulations. For example, operational ash dispersion forecasts require as input the MER and plume height (Folch, 2012), and typically the plume height is observed or imposed and a consistent MER estimate is required (e.g. Folch, 2012; Jenkins et al., 2015; Beckett et al., 2020). In probabilistic tephra modelling, scenarios are often based on eruption magnitude (e.g. Bonadonna et al., 2005; Bear-Crozier et al., 2016; Tadini et al., 2022) from which an MER is imposed and a consistent plume height is determined.

In many cases the imposed explanatory variable is given without uncertainty, and the estimate of the response variable is typically derived directly from the best-fit curve. This approach neglects both uncertainties in the 'measured' variable and the uncertainty in the response variable due to the use of the observational dataset. Accounting for these uncertainties is important to ensure that results are not biased by application of the best-fit result. Tephra dispersion patterns are strongly influenced by the plume height (Devenish et al., 2012; Dioguardi et al., 2020; Pardini et al., 2022), particularly where there is significant atmospheric wind shear with altitude, while the concentrations of airborne tephra, or ground level loadings, depend on the MER.

The Bayesian linear regression used here provides a method to compute values of the response variable that are consistent with the imposed value of the explanatory variable, and associate probabilities with these (Q, H) pairs, by drawing samples from the posterior predictive distribution. As the statistical model provides an analytical posterior predictive distribution, we can readily draw random samples directly. Alternatively, we can use a structured sampling design, for example by drawing values of the response variable at specified percentiles, which can ensure that unusual (Q, H) pairs are included in an ensemble, with knowledge of their probability. Accessing the tails of the distribution is likely to be important to ensure that 'rare' events are included in ensembles. Knowledge of the probabilities of inputs allows ensemble members to be weighted appropriately when aggregating to create probabilistic outputs, reducing the need for large ensembles. These approaches allow quantitative uncertainty to be included in dispersion modelling.

In forecasting applications, the uncertainty in both the observed plume height and inferred MER can be quantified using the Bayesian linear regression. Specifically, imposing a proper probability distribution for the plume height observation to represent its measurement uncertainty, and sampling from the joint posterior predictive distribution allows a set of (Q, H) pairs to be constructed as inputs for an ensemble of dispersion simulations. This could be combined with meteorological and other eruption source parameter uncertainty (Beckett, Witham, Hort, Stevenson, Bonadonna and Millington, 2015; Osman, Beckett, Rust and Snee, 2020, e.g.,) to create probabilistic airborne ash dispersion forecasts. In Williams et al. (2024) we show how the analytical form of the posterior predictive distribution can be used to efficiently generate probabilistic volcanic ash hazard forecasts that incorporate uncertainty in eruption source parameters and meteorological fields.

5. Conclusion

Eruption source parameter datasets are valuable catalogues of past eruptions. Relationships derived from these datasets provide useful tools that can be rapidly deployed during response to eruption, or used to inform preparedness. However, the aleatoric and epistemic uncertainties captured within the datasets propagate through curve fits into methods that adopt these expressions. By applying Bayesian linear regression, these uncertainties can be quantified, providing new capability for probabilistic approaches that adopt these relationships.

The expansion of eruption source parameter dataset provides new insights into the controls on plume dynamics (Aubry et al., 2021, 2023). With increasing numbers of events in the catalogue, more of nature's variations are recorded, so it is not surprising that we observe increased scatter around the simplest MER–plume height relationship. Including additional explanatory variables may improve a model's predictive capability by reducing epistemic uncertainty, but this is tensioned by the increased demand to measure and specify variables when applying models. The increased complexity of multi-variable modelling must be considered carefully against the improvement in prediction. In this regard Bayesian approach are particularly useful, with quantitative methods for comparing competing models.

Analysis of the eruption source parameter datasets to derive simple relationships facilitates rapid response hazard modelling by allowing variables that are difficult to determine to be inferred from easily measure quantities. Bayesian approaches are likely to provide useful tools for this analysis, but providing meaningful and useful uncertainty quantification.

Acknowledgements

I am indebted to Prof. Jonathan Rougier (University of Bristol and Rougier Consulting Ltd) for inspiring my interest in Bayesian statistics which initiated this work. I am also grateful for the enthusiastic support for this work from Prof. Jeremy Phillips (University of Bristol), Dr Frances Beckett (Met Office), Prof. Anthony Lee (University of Bristol) and Shannon Williams (University of Bristol); their helpful suggestions have greatly improved this study. I acknowledge funding from NERC for the VolcTools project (NE/R003890/1), and from EPSRC through the University of Bristol's impact acceleration account.

References

Abril-Pla, O., Andreani, V., Carroll, C., Dong, L., Fonnesbeck, C.J., Kochurov, M., Kumar, R., Lao, J., Luhmann, C.C., Martin, O.A., Osthege, M., Vieira, R., Wiecki, T., Zinkov, R., 2023. PyMC: A modern, and comprehensive probabilistic programming framework in Python. PeerJ Computer Science 9, e1516. doi:10.7717/peerj-cs.1516.

Aubry, T.J., Engwell, S., Bonadonna, C., Carazzo, G., Scollo, S., Van Eaton, A.R., Taylor, I.A., Jessop, D., Eychenne, J., Gouhier, M., Mastin, L.G., Wallace, K.L., Biass, S., Bursik, M., G., G.R., Jellinek, A.M., Schmidt, A., 2021. The Independent Volcanic Eruption Source Parameter Archive (IVESPA, version 1.0): A new observational dataset to support explosive eruptive column model validation and development. J Volcanol Geothermal Res 417, 107295. doi:10.106/j.jvolgeores.2021.107295.

Aubry, T.J., Engwell, S.L., Bonadonna, C., Mastin, L.G., Carazzo, G., Van Eaton, A.R., Jessop, D.E., Grainger, R.G., Scollo, S., Taylor, I.A., Jellinek, A.M., Schmidt, A., Biass, S., Gouhier, M., 2023. New Insights Into the Relationship Between Mass Eruption Rate and Volcanic Column Height Based On the IVESPA Data Set. Geophysical Research Letters 50, e2022GL102633. doi:10.1029/2022GL102633.

Bear-Crozier, A.N., Miller, V., Newey, V., Horspool, N., Weber, R., 2016. Probabilistic Volcanic Ash Hazard Analysis (PVAHA) I: Development of the VAPAH tool for emulating multi-scale volcanic ash fall analysis. Journal of Applied Volcanology 5, 3. doi:10.1186/s13617-016-0043-4.

Beckett, F.M., Witham, C.S., Hort, M.C., Stevenson, J.A., Bonadonna, C., Millington, S.C., 2015. Sensitivity of dispersion model forecasts of volcanic ash clouds to the physical characteristics of the particles. Journal of Geophysical Research: Atmospheres 120. doi:10.1002/2015JD023609.

Beckett, F.M., Witham, C.S., Leadbetter, S.J., Crocker, R., Webster, H.N., Hort, M.C., Jones, A.R., Devenish, B.J., Thomson, D.J., 2020. Atmospheric Dispersion Modelling at the London VAAC: A Review of Developments since the 2010 Eyjafjallajökull Volcano Ash Cloud. Atmosphere 11, 352. doi:10.3390/atmos11040352.

Bonadonna, C., Connor, C.B., Houghton, B.F., Connor, L., Byrne, M., Laing, A., Hincks, T.K., 2005. Probabilistic modeling of tephra dispersal: Hazard assessment of a multiphase rhyolitic eruption at Tarawera, New Zealand. Journal of Geophysical Research: Solid Earth 110, 2003JB002896. doi:10.1029/2003JB002896.

Bonadonna, C., Costa, A., 2013. Plume height, volume, and classification of explosive volcanic eruptions based on the Weibull function. Bulletin of Volcanology 75, 1–19. doi:10.1007/s00445-013-0742-1.

Bursik, M., 2001. Effect of wind on the rise height of volcanic plumes. Geophysical research letters 28, 3621–3624. doi:10.1029/2001GL013393.

Chaloner, K., Brant, R., 1988. A Bayesian approach to outlier detection and residual analysis. Biometrika 75, 651–659. doi:10.1093/biomet/75.4.651.

Degruyter, W., Bonadonna, C., 2012. Improving on mass flow rate estimates of volcanic eruptions. Geophysical research letters 39, L16308. doi:10.1029/2012GL052566 10.1029/2012GL052566.

Devenish, B.J., Francis, P.N., Johnson, B.T., Sparks, R.S.J., Thomson, D.J., 2012. Sensitivity analysis of dispersion modeling of volcanic ash from Eyjafjallajökull in May 2010. Journal of Geophysical Research: Atmospheres 117, 2011JD016782. doi:10.1029/2011JD016782.

Dioguardi, F., Beckett, F., Dürig, T., Stevenson, J.A., 2020. The Impact of Eruption Source Parameter Uncertainties on Ash Dispersion Forecasts During Explosive Volcanic Eruptions. Journal of Geophysical Research: Atmospheres 125, e2020JD032717. doi:10.1029/2020JD032717.

Folch, A., 2012. A review of tephra transport and dispersal models: Evolution, current status, and future perspectives. Journal of Volcanology and Geothermal Research 235–236, 96–115. doi:10.1016/j.jvolgeores.2012.05.020.

Gelman, A., Carlin, J., Stern, H., Dunson, D., Vehtari, A., Rubin, D., 2014. Bayesian Data Analysis. Texts in Statistical Science. 3 ed., CRC Press/Taylor and Francis, Boca Raton, FL.

Global Volcanism Program, 2023. [Database] Volcanoes of the World (v. 5.1.5; 15 Dec 2023). Distributed by Smithsonian Institution, compiled by Venzke, E. https://doi.org/10.5479/si.GVP.VOTW5-2023.5.1.

Jenkins, S.F., Barsotti, S., Hincks, T.K., Neri, A., Phillips, J.C., Sparks, R.S.J., Sheldrake, T., Vougioukalakis, G., 2015. Rapid emergency assessment of ash and gas hazard for future eruptions at Santorini Volcano, Greece. Journal of Applied Volcanology 4, 16. doi:10.1186/s13617-015-0033-y.

Lu, D., Ye, M., Hill, M.C., 2012. Analysis of regression confidence intervals and Bayesian credible intervals for uncertainty quantification. Water Resources Research 48, 2011WR011289. doi:10.1029/2011WR011289.

Mastin, L.G., Guffanti, M., Servranckx, R., Webley, P., Barsotti, S., Dean, K., Durant, A., Ewert, J.W., Neri, A., Rose, W.I., Schneider, D., Siebert, L., Stunder, B., Swanson, G., Tupper, A., Volentik, A., Waythomas, C.F., 2009. A multidisciplinary effort to assign realistic source parameters to models of volcanic ash-cloud transport and dispersion during eruptions. Journal of Volcanology and Geothermal Research 186, 10–21. doi:10.1016/j.jvolgeores.2009.01.008.

Morton, B.R., Taylor, G., Turner, J.S., 1956. Turbulent gravitational convection from maintained and instantaneous sources. Proceedings of The Royal Society of London Series A-mathematical Physical and Engineering Sciences 234, 1–23. doi:10.1098/rspa.1956.0011.

Osman, S., Beckett, F., Rust, A., Snee, E., 2020. Sensitivity of Volcanic Ash Dispersion Modelling to Input Grain Size Distribution Based on Hydromagmatic and Magmatic Deposits. Atmosphere 11, 567. doi:10.3390/atmos11060567.

Pardini, F., De' Michieli Vitturi, M., Andronico, D., Esposti Ongaro, T., Cristaldi, A., Neri, A., 2022. Real-time probabilistic assessment of volcanic hazard for tephra dispersal and fallout at Mt. Etna: The 2021 lava fountain episodes. Bulletin of Volcanology 85, 6. doi:10.1007/s00445-022-01614-z.

Pyle, D.M., 2015. Chapter 13 - sizes of volcanic eruptions, in: Sigurdsson, H. (Ed.), The Encyclopedia of Volcanoes (Second Edition). second edition ed.. Academic Press, Amsterdam, pp. 257–264. doi:http://dx.doi.org/10.1016/B978-0-12-385938-9.00013-4.

Rasmussen, C.E., Williams, C.K.I., 2006. Gaussian Processes for Machine Learning. Adaptive Computation and Machine Learning, MIT Press, Cambridge, Mass.

Settle, M., 1978. Volcanic eruption clouds and the thermal power output of explosive eruptions. Journal of Volcanology and Geothermal Research 3, 309–324. doi:10.1016/0377-0273(78)90041-0.

Sparks, R.S.J., 1986. The dimensions and dynamics of volcanic eruption columns. Bulletin of Volcanology 48, 3–15. doi:10.1007/BF01073509.

Sparks, R.S.J., Bursik, M.I., Carey, S.N., Gilbert, J.S., Glaze, L.S., Sigurdsson, H., Woods, A.W., 1997. Volcanic Plumes. John Wileys & Sons, Chichester, U.K.

Sparks, S.R.J., Aspinall, W.P., Barclay, J., Renfrew, I.A., Contreras-Arratia, R., Stewart, R., 2024. Analysis of magma flux and eruption intensity during the 2021 explosive activity at La Soufrière, St Vincent, West Indies. Geological Society, London, Special Publications 539, 63–79. doi:10.1144/SP539-2022-286.

Stan Development Team, 2023. Stan Modeling Language Users Guide and Reference Manual, Version 2.34. https://mc-stan.org.

Tadini, A., Azzaoui, N., Roche, O., Samaniego, P., Bernard, B., Bevilacqua, A., Hidalgo, S., Guillin, A., Gouhier, M., 2022. Tephra Fallout Probabilistic Hazard Maps for Cotopaxi and Guagua Pichincha Volcanoes (Ecuador)

With Uncertainty Quantification. Journal of Geophysical Research: Solid Earth 127, e2021JB022780. doi:10.1029/2021JB022780.

Walker, G., 1980. The Taupo pumice: Product of the most powerful known (ultraplinian) eruption? Journal of Volcanology and Geothermal Research 8, 69–94. doi:http://dx.doi.org/10.1016/0377-0273(80)90008-6.

Williams, S., Beckett, F., Leadbetter, S.J., Phillips, J.C., Lee, A., Woodhouse, M.J., 2024. Incorporating eruption source parameter and meteorological variability in the generation of probabilistic volcanic ash hazard forecasts. In prep. .

Wilson, L., Sparks, R.S.J., Huang, T.C., Watkins, N.D., 1978. The control of volcanic column heights by eruption energetics and dynamics. Journal of geophysical research 83, 1829–1836. doi:10.1029/JB083iB04p01829.

Woodhouse, M.J., Hogg, A.J., Phillips, J.C., Sparks, R.S.J., 2013. Interaction between volcanic plumes and wind during the 2010 Eyjafjallajökull eruption, Iceland. Journal of geophysical research 118, 92–109. doi:10.1029/2012JB009592.

Woods, A.W., 1988. The fluid dynamics and thermodynamics of eruption columns. Bulletin of Volcanology 50, 169–193. doi:10.1007/BF01079681.